



34 Chaulet et al., 2012; Seddik et al., 2012; Enderlin et al., 2014). Thus long-term accurate velocity measurements remain
35 fundamental to refining uncertainties in the estimates of mass balance of the Antarctic Ice Sheet.

36
37 As the largest ice shelf in East Antarctic Ice Sheet, the Amery Ice Shelf (AIS) buttresses the Lambert Glacier Basin
38 which constitutes the fourth largest drainage system in Antarctica (Giovinetto, 1964; McIntyre, 1985) draining
39 approximately 12.5% of the Antarctic Ice Sheet (Drewry, 1983). Lambert Glacier and other two primary tributary
40 glaciers transport ice from the interior Lambert Glacier Basin through the southern grounding line of the AIS
41 discharging into the Prydz Bay. This large drainage area occupies only 2.5% of the East Antarctic coastline (Fricker
42 et al., 2000) making AIS a sensitive indicator to mass balance change of the East Antarctic Ice Sheet. Furthermore,
43 due to the fast ice flows are primarily located along the southern segments of the AIS grounding line this area becomes
44 an important ice fluxgate to monitor the majority of ice mass redistribution into the AIS.

45
46 Remote sensing has revolutionized our ability to observe and measure surface velocities over vast areas with high
47 spatial resolution and has provided the comprehensive observations needed for modern scientific investigations of ice
48 dynamics and mass balance. Many early surface velocity estimates were made by expensive field survey
49 measurements (Stephenson and Bindshadler, 1994; Frezzotti et al., 1998). Field survey techniques, particularly with
50 the usage of Global Positioning System (GPS), have been used later (Manson et al., 2000; Sunil et al., 2007; Zhang et
51 al., 2008), but remain logistical difficulty in accessing remote portions of Antarctica and make them expensive to
52 obtain (Yang et al., 2014). Recent decades have seen the benefit from the advent of interferometric SAR (InSAR)
53 which enables accurate surface motion detection over large areas (Goldstein et al., 1993; Rosen et al., 2000; Joughin,
54 2002; Young & Hyland, 2002; Yu, 2005; Tang, 2007). However, successful InSAR measurements remain highly
55 dependent on the data acquisition, topographic characteristics, and coherence of SAR image pairs.

56
57 Feature tracking is a widely used image-based technique which tracks the motion of distinctive surface features
58 moving with the ice and persistent in image pairs acquired by space-borne optical instruments over time (Gray et al.,
59 1998). Successfully tracking the motion of small surface features through cross-correlation (Bindshadler et al., 1994;
60 Berthier et al., 2003; Stearns and Hamilton, 2005; Fahnestock et al., 2016) requires that the same feature be detected
61 reliably and consistently across sequential images. The extremely frozen environment in Antarctica enables to retain
62 consistent surface features well on the ground surface, which is suitable for a feature tracking approach.

63
64 Comprising the largest glacier-ice shelf system in East Antarctica, three tributary glaciers along with the AIS have
65 been investigated by surface velocity mapping (Joughin, 2002; Yu et al., 2010; Pittard et al., 2012; Pittard et al., 2015).
66 However, the surface velocity variations in the AIS have been relatively undocumented, with limited research
67 suggesting a stable surface velocity distribution and no loss of ice mass exhibit in the AIS (Pittard et al., 2015; Pittard
68 et al., 2017). This study uses feature tracking to investigate the inter-annual and intra-annual surface velocity variations
69 along the southern grounding line of AIS. Here surface velocities are measured for five consecutive austral summers
70 and winters between 2014 and 2018.



71 **2 Study Area**

72 The AIS (Fig 1) is geographically located in East Antarctica spanning approximately 68.5°S to 81°S latitude and 40°E
73 to 95°E longitude (Fricker et al., 2000). The Lambert, Mellor, and Fisher Glaciers originate farthest inland, flow
74 northward, and form a confluence zone discharging to AIS through the fluxgate between the Prince Charles Mountains
75 and the Mawson Escarpment (Hambrey, 1991; Yu, 2005). The southern grounding line is the location of the ice
76 fluxgate connecting the interior Lambert Glacier Basin with a large embayment northward of Prydz Bay.

77 **3 Data Preparation**

78 The Landsat-8 satellite was successfully launched by the National Aeronautics and Space Administration (NASA) in
79 2013 with the orbit height of 705 km, the orbital inclination of 98.2°, the orbital period of 98.2 minutes, and an 8-day
80 revisit cycle. Its Operational Land Imager (OLI) image product consists of 7 spectral bands at 30 m and a panchromatic
81 band (band 8) at 15 m spatial resolution respectively. Provided by the United States Geological Survey (USGS), the
82 Landsat-8 L1GT product has been co-registered with the high-resolution Radarsat Antarctic Mapping Project (RAMP)
83 Version 2 DEM to enable systematic geometric terrain correction (USGS, 2019) and was used in this study. The L1GT
84 product is stored as 16-bit signed integers.

85

86 Ten image pairs constructed from twenty cloud free images (Table 1) were used to derive the surface velocities for
87 the consecutive austral summers and winters during 2014–2018. An additional cloud free image pair was used to
88 derive the latest surface velocity for 2019 along with the determination of the locations of the ends of the southern
89 grounding line segments of the AIS used in this study. Winter is defined as July–October and summer as January–
90 March. The preferred temporal interval for each image pair is one month but the actual time separation varies slightly
91 due to the data availability. All images were processed using Environment for Visualizing Images (ENVI5.5) software
92 package supplemented an installation of the Co-registration of Optically Sensed Images and Correlation (Cosi-Corr)
93 program (Leprince et al., 2007).

94

95 In this study, the grounding line was determined by the Mosaic of Antarctica (MOA) 2008–2009 mission (Haran et
96 al., 2014). This MOA grounding line product was generated using the composited Moderate Resolution Imaging
97 Spectroradiometer (MODIS) image data acquired during the 2009 austral summer. The ice velocity and Antarctic
98 basin boundary were provided by the Making Earth System Data Records for Use in Research Environments
99 (MEaSURES) program. The MEaSURES surface velocities Version 2 (Rignot et al., 2017) observed in the study area
100 were an InSAR-based multiyear average velocity during 1996–2016.

101 **4 Methods**

102 As illustrated in Fig 2, feature tracking is based on an image-to-image cross-correlation algorithm which locates the
103 identical surface features from sequential images and measures their displacements in the frequency domain
104 (Bindschadler & Scambos, 1991; Scambos et al., 1992). This algorithm assumes: (1) a pre-event image (reference



105 image) plus a shift translation comprising a post-event image (search image); (2) the reference image and its paired
106 search image are assumed to share the same ground resolution and (3) are geolocated.

107

108 Surface features are represented by the patterns of a group of individual pixels. By shifting a 64 x 64 pixel search
109 window across the images in a pair (Ayoub et al., 2009b) every 4 pixels, the displacement of the dominant feature
110 within the window is computed through the normalized covariance correlation method (Bernstein, 1983). In the same
111 corresponding central pixel, the north-south (N/S) and east-west (E/W) components of the correlation are recorded, as
112 well as the signal-to-noise ratio (SNR), which is taken as the ratio of peak correlation function to the average value.

113

114 Given by two motion estimate components, N/S and E/W, the surface velocity can be calculated using Eq. (1):

$$115 \quad v = SQRT(NS^2 + EW^2)/t \quad (1)$$

116 where v represents the surface velocity magnitude estimate, $SQRT(NS^2 + EW^2)$ is the displacement magnitude, and t
117 represents the time interval between acquisition dates.

118

119 Due to providing sharp surface texture at 15 m resolution the Landsat-8 OLI band 8 imagery was used for feature
120 tracking. Preprocessing included applying a 3x3 Gaussian high pass filter to enhance the distinct surface features from
121 the panchromatic band 8 for both reference and search images. The Cosi-Corr software package was implemented to
122 accomplish the feature tracking procedures. This software package is a robust feature tracking program to obtain
123 surface velocity measurements and is available from the Caltech Tectonics Observatory website
124 (<http://www.tectonics.caltech.edu/>). Full details of the package can be found in Leprince et al (2007).

125

126 A set of location reference points were generated at 0.1 km intervals along the ~76 km AIS grounding line to facilitate
127 the monitoring of surface velocity variations as well as the accuracy and uncertainty assessments. Surface velocity
128 measurements were extracted using the geographic coordinates of the location reference points. The accuracy of the
129 surface velocity measurements was assessed using signal-to-noise (SNR) ratio as SNR value refers to the correlation
130 between the image window and the search window (Ayoub et al., 2009b). The SNR value of 1 represents the two
131 windows are perfectly correlated, while the SNR value of 0 shows no correlation.

132

133 All the computed velocities were passed through a quality control procedure to reduce possible miscorrelated
134 estimations. Any magnitude variation greater than 5% was considered to be an outlier and was disregarded in further
135 analysis. The magnitude variation was defined as the difference between the measurement and the mean of the two
136 adjacent measurements at the grounding line. Observation with low SNR (< 0.9) was omitted as well due to possible
137 miscorrelation.

138

139 Uncertainty analysis is fundamental to estimate the applicability of the determined surface velocity measurements.
140 Uncertainty of a single-pair velocity measurement is dominated by the accuracy of the feature tracking algorithm, the
141 co-registration of pre- and post- images, and the temporal variability of ice surface (Dehecq et al., 2015). The LIGHT



142 Landsat-8 OLI product used by this study has been applied with precision terrain correction and the uncertainty of
143 imagery co-registration has been minimized The uncertainty coming from the temporal variability of ice surface can
144 be negligible, since only the images with identical surface features in both pre- and post- images are used. Hence, the
145 uncertainty of the feature tracking algorithm exhibits in all the final velocity measurements and needs to be assessed
146 quantitatively.

147

148 The velocity measurement uncertainty can be assessed through the observed shifts in stable zones (e.g. exposed rocks,
149 massif, etc). However, due to inconsistent acquisition angles and temporal changes, any difference (e.g. shadow and
150 illumination as illustrated in Fig 3) exhibiting between pre- and post-event images can cause a measurable
151 miscorrelation. Therefore a small stable ice surface located in the north end of a nunatak was used in this study for
152 uncertainty assessment as no motion in this stable area should occur. Fifty random locations were generated within
153 the boundary of the selected stable ice surface (indicated in red dot in Fig 3).

154 5. Results

155 5.1 Major Ice Stream Velocity Identification

156 From the MOA grounding line product, the two ends of the AIS's southern grounding line segment for this study were
157 established where the surface velocity decreased to 0.5 m/d, based on the surface velocity measurements for 2019 (Fig
158 4). The grounding line was divided into three segments according to the MEaSURES Antarctic basin boundaries
159 (Rignot et al., 2013) as illustrated in Fig 4A. The lengths of each segment are 35.6 km, 14.1 km, and 26.3 km for
160 Fisher Glacier, Mellor Glacier, and Lambert Glacier, respectively. The mean velocity along a 3 km long grounding
161 line centered on the peak velocity was then computed to represent the highest surface velocity observed for each
162 glacier. The analysis for each individual glacier is discussed in section 5.4 is based on their average peak velocity as
163 illustrated in Fig 4B.

164 5.2 Inter-annual Surface Velocity Variations

165 Using feature tracking applied to Landsat-8 OLI band 8 image pairs, ice surface summer and winter velocities were
166 measured annually from 2014–2018. Each velocity measurement was generated using a pair of preprocessed pre- and
167 post-event images and represents an average surface velocity during the image acquisition interval.

168

169 The annual surface velocity was determined as the mean of the corresponding summer and winter velocities for each
170 year. The inter-annual variation was calculated by the surface velocity difference of the latter year and prior year over
171 the prior year velocity. A positive inter-annual variation indicates a surface velocity increase and vice versa.

172

173 Overall, the surface velocities across all three glaciers show a consistent ~ 5% inter-annual increase over the study
174 period (Fig 5). The multiyear mean surface velocities of Fisher Glacier, Mellor Glacier, and Lambert Glacier were
175 1.31, 1.93, and 2.17 m/d respectively during 2014–2018. The inter-annual surface velocity increased on average
176 0.09 ± 0.02 m/d (equivalent to 6.5%) over the study period (Table 2). All the three glaciers exhibited on average inter-



177 annual surface velocity increase, which was 0.08 ± 0.02 m/d, 0.10 ± 0.02 m/d, and 0.10 ± 0.03 m/d for Fisher, Mellor, and
178 Lambert Glaciers, respectively. Most of the inter-annual surface velocity increase of Mellor Glacier was from a large
179 inter-annual increase of ~ 0.31 m/d during 2014/2015.

180 **5.3 Intra-annual Surface Velocity Variations**

181 Two additional parameters, intra-annual variation and inter-seasonal variation, were calculated for each individual
182 glacier describing its surface velocity variations. Intra-annual variation is defined as the velocity variation calculated
183 by the summer-winter surface velocity difference over the summer surface velocity. A negative intra-annual variation
184 indicates the winter velocity is less than the summer velocity and vice versa. Inter-seasonal variation is defined as the
185 velocity variation calculated in percentage by the surface velocity difference between the current season (winter or
186 summer) and the prior season (summer or winter) over the current season's velocity. A positive inter-seasonal variation
187 represents the current season velocity is higher than the prior season velocity and vice versa.

188

189 The multiyear mean measurements indicate that on average surface velocities for winters and summers are similar
190 (Fig 6A). In addition to the changes in magnitude, the spatial pattern of velocity varied over the study period as well.
191 While the spatial pattern of surface velocities across the grounding lines of Fisher and Mellor Glaciers were generally
192 uniform both inter- and intra-annually, two regions of increased velocity appeared along the Lambert Glacier's
193 grounding line during the summer of 2018 (Fig 6B).

194

195 Except for 2016 and 2018, consistent variations in surface velocity were observed for Fisher Glacier and Mellor
196 Glacier with the winter surface velocity being higher than the summer velocity (Fig 6C). The winter surface velocity
197 of Lambert Glacier was faster than the summer surface velocity for two consecutive years and then declined in 2018.
198 While the surface velocities of Fisher Glacier and Mellor Glacier were higher in winter than in summer of 2018, the
199 opposite was true for Lambert Glacier. A significant inter-seasonal surface velocity increase was observed between
200 2014 winter and 2015 summer for all the three studied glaciers, while the largest increase of 64.3% was observed in
201 Fisher Glacier. An increase in inter-seasonal surface velocity was observed again in the summer of 2018 at Lambert
202 Glacier.

203

204 On average the intra-annual surface velocity variation was -0.06 ± 0.10 m/d over the study period, indicating slightly
205 lower average surface velocity in winter of approximately 3.13% (Table 3). The average intra-annual surface velocity
206 variation of Fisher Glacier, Mellor Glacier, and Lambert Glacier was small at -0.08 ± 0.06 m/d, -0.02 ± 0.09 m/d, and
207 -0.07 ± 0.14 m/d respectively. This is consistent with the overall increase in velocities over the study period. Most of
208 the intra-annual surface velocity variation was contributed by Fisher Glacier due to its large intra-annual surface
209 velocity variation of -0.42 ± 0.04 m/d in 2015. A positive intra-annual surface velocity variation was observed in 2016
210 and 2018 for all the three studied glaciers, which indicates the glaciers may even flow faster in winter than in summer
211 for these two years.

212 **5.4 Individual Glacier Analysis**



213 Since the surface velocity of each glacier varies considerably along the grounding line, the surface velocities for the
214 fastest moving segments are underrepresented by the average surface velocity over the entire grounding line.
215 Therefore, the average surface velocity at the peak location (illustrated in Fig 4) was computed and used to investigate
216 the inter-annual variation for each individual glacier. The inter-annual variation was converted into percentage by
217 dividing the prior surface velocity measurement. Annual surface velocities were generally stable across the three
218 studied glaciers (Fig 7A), but the inter-annual variation revealed a clear surface velocity decline during 2015/2016
219 (Fig 7B).

220

221 Although flowing slower than the other two glaciers, the surface velocity of Fisher Glacier was found to have greater
222 intra-annual and inter-annual variability. The intra-annual surface velocity variation on average was $-5.41 \pm 5.65\%$,
223 which indicates lower winter than summer surface velocities (Table 4). However, the average intra-annual surface
224 velocity variation of Fisher Glacier was 6.86% , indicating that on average the annual surface velocity of Fisher Glacier
225 increased $8.56 \pm 4.36\%$ every year. The largest intra-annual surface velocity variation of Fisher Glacier was $-$
226 $30.32 \pm 4.51\%$ (-0.25 m/d) in 2015.

227

228 Mellor Glacier had intermediate flow velocities between the other two glaciers and the inter-annual surface velocity
229 increased $6.47 \pm 3.48\%$ (0.41 m/d) over the study period, which is the medium variation among three studied glaciers
230 and can be translated into a 150 m per year velocity increase. Also, compared with the other two glaciers, Mellor
231 Glacier had the smallest inter-annual surface velocity increase in the last few years, which was $2.96 \pm 3.48\%$ during
232 2016–2017 and $10.15 \pm 1.65\%$ during 2017–2018.

233

234 As the fastest flowing tributary glacier, Lambert Glacier possessed the largest multiyear average inter-annual surface
235 velocity, which was 2.17 m/d. There was only $-3.28 \pm 9.47\%$ intra-annual variation and $5.79 \pm 9.20\%$ inter-annual
236 increase of surface velocity observed in Lambert Glacier, which were the lowest of the three. However, the fastest
237 inter-annual increase of surface velocity with high uncertainty was found in Lambert Glacier in the last years of the
238 observation period, which was $7.73 \pm 7.75\%$ during 2016/2017 and $17.24 \pm 15.06\%$ during 2017/2018.

239 5.5 Accuracy and Uncertainty Assessments

240 The overall accuracy of feature tracking is approximately 96.5% , according to the accuracy analysis shown in Table
241 5. Besides a consistent high accuracy exhibiting over the studied time period, there is no significant differences in the
242 measured uncertainty between summers and winters.

243

244 A small stable ice surface adjacent to an exposed rock island (indicated in Fig 3) was selected for uncertainty
245 assessment due to its minimal illumination differences between images. Uncertainty assessment of the feature tracking
246 algorithm was conducted based on fifty random locations. The ‘box and whisker plot’ method was used to visualize
247 the uncertainty for each year and the average uncertainty along the N/S and E/W directions. A generally close
248 uncertainty was observed in each individual study year (Fig 8A). The overall uncertainty was 0.20 m/d, while the



249 overall uncertainty along the N/S and E/W directions are 0.00 ± 0.02 m/d and -0.04 ± 0.01 m/d respectively (positive
250 towards East and negative towards West; Fig 8B). As shown in Fig 8A, the largest uncertainty at 0.25 ± 0.01 m/d was
251 observed in 2014, while the smallest uncertainty at 0.15 ± 0.09 m/d exhibited in 2018. We investigated the contribution
252 of the measured magnitudes and directions of these uncertainties in our computed velocity and variability assessments
253 and found that they did not lead to any significant adjustments to our measurements.

254 **6 Discussion**

255 There is currently little relevant research documenting inter-annual and seasonal changes in the surface velocity in the
256 AIS. However, there are a number of studies documenting such inter-annual and seasonal variations elsewhere in East
257 Antarctica. A 9.9 m/yr (equivalent to 0.02 m/d) inter-annual increase in surface velocity was observed in Langhovde
258 Glacier, East Antarctica from 2008–2010 (Fukuda et al., 2014). Zhou et al. (2014) reported a 19% seasonal decrease
259 in surface velocity from summer to winter during 1996–2008 in Polar Record Glacier (PRG), East Antarctica, which
260 is a small outlet glacier on the east side of the AIS towards the southern shore of Prydz Bay (Liang et al., 2019). This
261 outlet glacier experienced velocity variations of up to 15% from 2005–2015 (Liang et al., 2019), which is equivalent
262 to a 1.5% inter-annual increase. In addition, Liang et al. (2019) also demonstrated up to 9% seasonal increase in
263 surface velocity between winter and summer in PRG, East Antarctica.

264
265 This research demonstrates that the primary tributary glaciers into the AIS exhibit inter-annual, intra-annual, and inter-
266 seasonal variations in surface velocity approaching $6.94\pm 5.68\%$, $-2.98\pm 6.67\%$, and $3.67\pm 9.82\%$, respectively, along
267 the grounding line over the five year period 2014–2018 which is consistent with previous studies. The uncertainty
268 remains high given the limited five-year comparison window. However, over this period there is an overall 0.09 ± 0.02
269 m/d increase in inter-annual surface velocity variation translating into a ~ 29 m per year velocity increase or
270 approximately a 5% increase in average velocity. The overall intra-annual surface velocity variation at -0.06 ± 0.02 m/d
271 shows that on average winter surface velocity is ~ 15 m per year slower than summer surface velocity. No obvious
272 velocity variations appear to exist between summers and winters from our multiyear average measurements. Overall,
273 a consistent inter-seasonal surface velocity variation has been observed across all the three glaciers excluding a 9.1%
274 decrease in velocity of Lambert Glacier from summer to winter in 2018. A significant surface velocity increase was
275 observed across all the three glaciers between 2014 winter and 2015 summer, including the largest 64.3% increase in
276 surface velocity in Fisher Glacier.

277
278 It appears that the areas along the grounding line experiencing the highest velocities are also most sensitive to the
279 inter-annual and intra-annual velocity variations than the average velocity across the entire ground line of the three
280 studied tributary glaciers. Fast moving ice flow is more sensitive to the local environmental changes compared to slow
281 moving ice flow as glacier flow speeds are known to be an important factor in governing glacier's response to the
282 local environmental changes (Scambos et al., 2004; Stearns et al., 2008; Davies et al., 2012). Fisher Glacier
283 experiences greater velocity variations than the other two tributary glaciers most probably due to its slower velocities
284 and smaller size.



285

286 Our measured velocities over the 2014–2018 period are in general agreement with previous published results (Rignot
287 et al., 2017) for earlier decades. While limited historic surface velocity variations from either InSAR or feature-
288 tracking, those that do exist are in general agreement with the surface velocity measurements we observed over our
289 five-year study. As illustrated in Fig 9A, a good agreement exhibited in both the magnitude and location of the peak
290 flow velocity for all the three glaciers.

291

292 Based on the limited observations, a surface velocity decline appeared from 1989 to the early 2000s which continued
293 through 2014. From 2014–2018 the surface velocities were found to increase. In 2018 the surface velocity was
294 generally close to the velocity observed in 1989 (Fig 9B) and the locations in peak flow velocities along the grounding
295 line particularly for Fisher Glacier and Lambert Glacier were largely unchanged. However, it is important to note that
296 the variations in velocity observed in this study between 2014 and 2018 encompass nearly as large a range in those
297 decadal differences observed from 1989 to present.

298 **7 Conclusions**

299 This study examines surface velocity variations of temporal and spatial distribution along the southern segment of the
300 AIS grounding line. Furthermore, feature tracking approach is suitable to determine the surface velocity in the study
301 area, achieving the accuracy comparable to the InSAR method.

302

303 The multiyear mean feature tracking-based surface velocity is 1.31, 1.93, and 2.17 m/d for Fisher Glacier, Mellor
304 Glacier, and Lambert Glacier respectively. This study reveals a ~ 5% (0.09 ± 0.02 m/d) annual increase during 2014–
305 2018. Lambert Glacier and Mellor Glacier exhibit higher average inter-annual surface velocity increase at ~ 0.10 m/d,
306 while Fisher Glacier showed the largest on average intra-annual surface velocity at -0.08 ± 0.06 m/d. The studied
307 glaciers flow in winter nearly the same fast as in summer with only 0.07 ± 0.14 m/d difference within each year which
308 is only 3% of their average annual velocity.

309

310 These observations indicate variability in velocities along these grounding lines, but over the five year study period
311 general stability in surface velocities were observed. As the variations in surface velocities observed for these three
312 major tributary glaciers over the study period of 2014–2018 are similar in magnitude to the range of velocities to that
313 of measured since 1989 of the AIS suggests caution needs to be applied when comparing limited measurements from
314 various decades. This also suggests the surface velocities along the grounding line of the major tributary glaciers of
315 the AIS have remained relatively stable since the late 1980s.

316 **Acknowledgements**

317 We are thankful for the National Snow & Ice Data Center (NSIDC) for publishing the grounding line data at
318 <https://nsidc.org/data/nsidc-0593>. We also would like to thank the USGS for making the Landsat archive freely
319 available at <http://earthexplorer.usgs.gov/>.



320 **References**

- 321 Ayoub, F., LePrince, S., & Avouac, J. P. (2009a). Co-registration and correlation of aerial photographs for ground
322 deformation measurements. *Isprs Journal of Photogrammetry and Remote Sensing*, 64(6), 551-560,
323 doi:10.1016/j.isprsjprs.2009.03.005
324
- 325 Ayoub, F., LePrince, S., & Keene, L. (2009b). User's guide to COSI-Corr: Co-registration of optically sensed images
326 and correlation. Retrieved from [http://www.tectonics.caltech.edu/slip_history/spot_coseis/pdf_files/cosi-](http://www.tectonics.caltech.edu/slip_history/spot_coseis/pdf_files/cosi-corr_guide.pdf)
327 [corr_guide.pdf](http://www.tectonics.caltech.edu/slip_history/spot_coseis/pdf_files/cosi-corr_guide.pdf)
328
- 329 Bernstein, R. (1983). Image geometry and rectification. In R. N. Colwell (Ed.), *Manual of Remote Sensing* (pp. 881-
330 884). Falls Church, VA: American Society of Photogrammetry.
331
- 332 Berthier, E., Raup, B., & Scambos, T. (2003). New velocity map and mass-balance estimate of Mertz Glacier, East
333 Antarctica, derived from Landsat sequential imagery. *Journal of Glaciology*, 49(167), 503-511, doi:
334 10.3189/172756503781830377.
335
- 336 Bindshadler, R. A., Fahnestock, M. A., Skvarca, P., & Scambos, T. A. (1994). Surface-Velocity Field of the Northern
337 Larsen Ice Shelf, Antarctica. *Annals of Glaciology*, Vol 20, 1994, 20, 319-326, doi: 10.3189/172756494794587294.
338
- 339 Chi, Z. (2012). Investigation of glacial dynamics in the Lambert Glacier-Amery Ice Shelf System (LAS) using remote
340 sensing. (PhD), Texas A&M University, College Station, TX.
341
- 342 Davies, B. J., Carrivick, J. L., Glasser, N. F., Hambrey, M. J., & Smellie, J. L. (2012). Variable glacier response to
343 atmospheric warming, northern Antarctic Peninsula, 1988-2009. *Cryosphere*, 6(5), 1031-1048, doi:10.5194/tc-6-
344 1031-2012.
345
- 346 Dehecq, A., Gourmelen, N., & Trouve, E. (2015). Deriving large-scale glacier velocities from a complete satellite
347 archive: Application to the Pamir-Karakoram-Himalaya. *Remote Sensing of Environment*, 162, 55-66,
348 doi:10.1016/j.rse.2015.01.031.
349
- 350 Drewry, D. J. (1983). *Antarctica: Glaciological and Geophysical Folio*. Cambridge, U.K.: Scott Polar Research
351 Institute, University of Cambridge.
352
- 353 Enderlin, E. M., Howat, I. M., Jeong, S., Noh, M. J., van Angelen, J. H., & van den Broeke, M. R. (2014). An improved
354 mass budget for the Greenland ice sheet. *Geophysical Research Letters*, 41(3), 866-872, doi:10.1002/2013gl059010.
355



- 356 Fahnestock, M., Scambos, T., Moon, T., Gardner, A., Haran, T., & Klinger, M. (2016). Rapid large-area mapping of
357 ice flow using Landsat 8. *Remote Sensing of Environment*, 185, 84-94, doi:10.1016/j.rse.2015.11.023.
358
- 359 Frezzotti, M., Capra, A., & Vittuari, L. (1998). Comparison between glacier ice velocities inferred from GPS and
360 sequential satellite images. *Annals of Glaciology*, Vol 27, 1998, 27, 54-60.
361
- 362 Fricker, H. A., Warner, R. C., & Allison, I. (2000). Mass balance of the Lambert Glacier-Amery Ice Shelf system,
363 East Antarctica: a comparison of computed balance fluxes and measured fluxes. *Journal of Glaciology*, 46(155), 561-
364 570, doi: 10.3189/172756500781832765.
365
- 366 Fukuda, T., Sugiyama, S., Sawagaki, T., & Nakamura, K. (2014). Recent variations in the terminus position, ice
367 velocity and surface elevation of Langhovde Glacier, East Antarctica. *Antarctic Science*, 26(6), 636-645,
368 doi:10.1017/S0954102014000364.
369
- 370 Gillet-Chaulet, F., Gagliardini, O., Seddik, H., Nodet, M., Durand, G., Ritz, C., Vaughan, D. G. (2012). Greenland ice
371 sheet contribution to sea-level rise from a new-generation ice-sheet model. *Cryosphere*, 6(6), 1561-1576,
372 doi:10.5194/tc-6-1561-2012.
373
- 374 Giovinetto, M. B. (1964). The drainage systems of Antarctica: Accumulation. Paper presented at the AGU,
375 Washington, D.C.
376
- 377 Goldstein, R. M., Engelhardt, H., Kamb, B., & Frolich, R. M. (1993). Satellite Radar Interferometry for Monitoring
378 Ice-Sheet Motion - Application to an Antarctic Ice Stream. *Science*, 262(5139), 1525-1530, doi:
379 10.1126/science.262.5139.1525.
380
- 381 Gray, A. L., Mattar, K. E., Vachon, P. W., Bindschadler, R., Jezek, K. C., Forster, R., & Crawford, J. P. (1998). InSAR
382 results from the RADARSAT Antarctic Mapping Mission data: Estimation of glacier motion using a simple
383 registration procedure. *Igarss '98 - 1998 International Geoscience and Remote Sensing Symposium, Proceedings Vols*
384 *1-5*, 1638-1640, doi: 10.1109/Igarss.1998.691662.
385
- 386 Hambrey, M. J. (1991). Structure and dynamics of the Lambert Glacier-Amery Ice Shelf System: implications for the
387 origin of Prydz Bay sediments.
388
- 389 Haran, T., Bohlander, J. A., Scambos, T., Painter, T., & Fahnestock, M. (2014). MODIS Mosaic of Antarctica 2008-
390 2009 (MOA2009) Image Map, Version 1. Boulder, Colorado.
391
- 392 IPCC. (2007). *Climate change 2007: Mitigation*. Retrieved from Cambridge, United Kingdom.



- 393
394 IPCC. (2013). Summary for policymakers. Retrieved from Cambridge, United Kingdom.
395
396 Joughin, I. (2002). Ice-sheet velocity mapping: a combined interferometric and speckle-tracking approach. *Annals of*
397 *Glaciology*, Vol 34, 2002, 34, 195-201, doi: 10.3189/172756402781817978.
398
399 Leprince, S., Barbot, S., Ayoub, F., & Avouac, J. P. (2007). Automatic and precise orthorectification, coregistration,
400 and subpixel correlation of satellite images, application to ground deformation measurements. *IEEE Transactions on*
401 *Geoscience and Remote Sensing*, 45(6), 1529-1558, doi:10.1109/Tgrs.2006.888937.
402
403 Liang, Q., Zhou, C., Howat, I., Jeong, S., Liu, R., & Chen, Y. (2019). Ice flow variations at Polar Record Glacier, East
404 Antarctica. *Journal of Glaciology*, 65(250), 279-287, doi:10.1017/jog.2019.6
405
406 Manson, R., Coleman, R., Morgan, P., & King, M. (2000). Ice velocities of the Lambert Glacier from static GPS
407 observations. *Earth Planets and Space*, 52(11), 1031-1036, doi: 10.1186/Bf03352326.
408
409 McIntyre, N. F. (1985). A Re-Assessment of the Mass Balance of the Lambert Glacier Drainage-Basin, Antarctica.
410 *Journal of Glaciology*, 31(107), 34-38, doi: 10.3189/S0022143000004962.
411
412 Miles, B. W. J., Stokes, C. R., Vieli, A., & Cox, N. J. (2013). Rapid, climate-driven changes in outlet glaciers on the
413 Pacific coast of East Antarctica. *Nature*, 500(7464), doi:10.1038/nature12382.
414
415 Pittard, M. L., Galton-Fenzi, B. K., Watson, C. S., & Roberts, J. L. (2017). Future sea level change from Antarctica's
416 Lambert-Amery glacial system. *Geophysical Research Letters*, 44(14), 7347-7355, doi:10.1002/2017gl073486.
417
418 Pittard, M. L., Roberts, J. L., Warner, R. C., Galton-Fenzi, B. K., Watson, C. S., & Coleman, R. (2012). Flow of the
419 Amery Ice Shelf and its tributary glaciers. Paper presented at the In 18th Australasian Fluid Mechanics Conference,
420 Launceston, Australia.
421
422 Pittard, M. L., Roberts, J. L., Watson, C. S., Galton-Fenzi, B. K., Warner, R. C., & Coleman, R. (2015). Velocities of
423 the Amery Ice Shelf's primary tributary glaciers, 2004-12. *Antarctic Science*, 27(5), 511-523,
424 doi:10.1017/S0954102015000231.
425
426 Pritchard, H. D., Ligtenberg, S. R. M., Fricker, H. A., Vaughan, D. G., van den Broeke, M. R., & Padman, L. (2012).
427 Antarctic ice-sheet loss driven by basal melting of ice shelves. *Nature*, 484(7395), 502-505, doi:10.1038/nature10968.
428



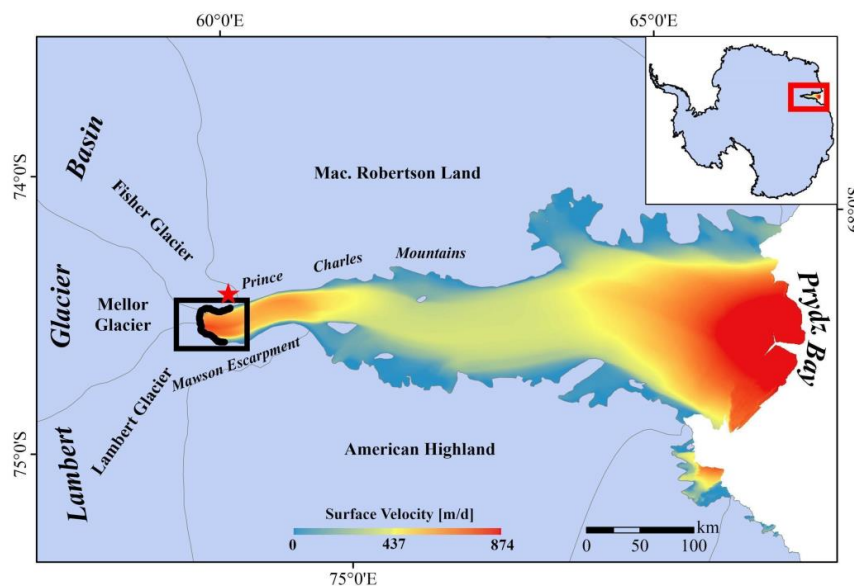
- 429 Rignot, E., Bamber, J. L., Van Den Broeke, M. R., Davis, C., Li, Y. H., Van De Berg, W. J., & Van Meijgaard, E.
430 (2008). Recent Antarctic ice mass loss from radar interferometry and regional climate modelling. *Nature Geoscience*,
431 1(2), 106-110, doi:10.1038/ngeo102.
- 432
- 433 Rignot, E., Casassa, G., Gogineni, P., Krabill, W., Rivera, A., & Thomas, R. (2004). Accelerated ice discharge from
434 the Antarctic Peninsula following the collapse of Larsen B ice shelf. *Geophysical Research Letters*, 31(18), doi:Artn
435 L1840110.1029/2004gl020697.
- 436
- 437 Rignot, E., & Kanagaratnam, P. (2006). Changes in the velocity structure of the Greenland ice sheet. *Science*,
438 311(5763), 986-990, doi:10.1126/science.1121381.
- 439
- 440 Rignot, E., Mouginot, J., & B., S. (2017). MEaSURES InSAR-Based Antarctica Ice Velocity Map, Version 2. Boulder,
441 Colorado.
- 442 Rignot, E., Velicogna, I., van den Broeke, M. R., Monaghan, A., & Lenaerts, J. (2011b). Acceleration of the
443 contribution of the Greenland and Antarctic ice sheets to sea level rise. *Geophysical Research Letters*, 38, doi:Artn
444 L0550310.1029/2011gl046583.
- 445
- 446 Rosen, P. A., Hensley, S., Joughin, I. R., Li, F. K., Madsen, S. N., Rodriguez, E., & Goldstein, R. M. (2000). Synthetic
447 aperture radar interferometry - Invited paper. *Proceedings of the Ieee*, 88(3), 333-382, doi: 10.1109/5.838084.
- 448
- 449 Scambos, T. A., Bohlander, J. A., Shuman, C. A., & Skvarca, P. (2004). Glacier acceleration and thinning after ice
450 shelf collapse in the Larsen B embayment, Antarctica. *Geophysical Research Letters*, 31(18), doi:Artn
451 L1840210.1029/2004gl020670.
- 452
- 453 Scambos, T. A., Dutkiewicz, M. J., Wilson, J. C., & Bindschadler, R. A. (1992). Application of Image Cross-
454 Correlation to the Measurement of Glacier Velocity Using Satellite Image Data. *Remote Sensing of Environment*,
455 42(3), 177-186, doi: 10.1016/0034-4257(92)90101-O.
- 456
- 457 Seddik, H., Greve, R., Zwinger, T., Gillet-Chaulet, F., & Gagliardini, O. (2012). Simulations of the Greenland ice
458 sheet 100 years into the future with the full Stokes model Elmer/Ice. *Journal of Glaciology*, 58(209), 427-440,
459 doi:10.3189/2012JoG11J177.
- 460
- 461 Shen, Q., Wang, H. S., Shum, C. K., Jiang, L. M., Hsu, H. T., & Dong, J. L. (2018). Recent high-resolution Antarctic
462 ice velocity maps reveal increased mass loss in Wilkes Land, East Antarctica. *Scientific Reports*, doi: 10.1038/s41598-
463 018-22765-0.
- 464



- 465 Stearns, L., & Hamilton, G. (2005). A new velocity map for Byrd Glacier, East Antarctica, from sequential ASTER
466 satellite imagery. *Annals of Glaciology*, Vol 41, 2005, 41, 71-76, doi: 10.3189/172756405781813393.
- 467
- 468 Stearns, L. A., Smith, B. E., & Hamilton, G. S. (2008). Increased flow speed on a large East Antarctic outlet glacier
469 caused by subglacial floods. *Nature Geoscience*, 1(12), 827-831, doi:10.1038/ngeo356.
- 470
- 471 Stephenson, S. N., & Bindschadler, R. A. (1988). Observed Velocity Fluctuations on a Major Antarctic Ice Stream.
472 *Nature*, 334(6184), 695-697, doi: 10.1038/334695a0.
- 473
- 474 Sunil, P. S., Reddy, C. D., Ponraj, M., Dhar, A., & Jayapaul, D. (2007). GPS determination of the velocity and strain-
475 rate fields on Schirmacher Glacier, central Dronning Maud Land, Antarctica. *Journal of Glaciology*, 53(183), 558-
476 564, doi: 10.3189/002214307784409199.
- 477
- 478 Tang, S. (2007). Investigation of coastal dynamics of the Antarctic ice sheet using sequential Radarsat SAR images.
479 (MS), Texas A&M University, College Station, TX.
- 480
- 481 USGS. (2019). Landsat Collection 1 Level Production Definition. Retrieved from [https://prd-wret.s3-us-west-](https://prd-wret.s3-us-west-2.amazonaws.com/assets/palladium/production/atoms/files/LSDS-1656%20Landsat%20Collection1%20L1%20Product%20Definition-v2.pdf)
482 [2.amazonaws.com/assets/palladium/production/atoms/files/LSDS-](https://prd-wret.s3-us-west-2.amazonaws.com/assets/palladium/production/atoms/files/LSDS-1656%20Landsat%20Collection1%20L1%20Product%20Definition-v2.pdf)
483 [1656 %20Landsat Collection1 L1 Product Definition-v2.pdf](https://prd-wret.s3-us-west-2.amazonaws.com/assets/palladium/production/atoms/files/LSDS-1656%20Landsat%20Collection1%20L1%20Product%20Definition-v2.pdf)
- 484
- 485 Yang, Y. D., Bo, S., Wang, Z. M., Ding, M. H., Hwang, C. W., Ai, S. T., . . . E, D. C. (2014). GPS-derived velocity
486 and strain fields around Dome Argus, Antarctica. *Journal of Glaciology*, 60(222), 735-742,
487 doi:10.3189/2014JoG14J078.
- 488
- 489 Young, N. W., & Hyland, G. (2002). Velocity and strain rates derived from InSAR analysis over the Amery Ice Shelf,
490 East Antarctica. *Annals of Glaciology*, Vol 34, 2002, 34, 228-234, doi: 10.3189/172756402781817842.
- 491
- 492 Yu, J. (2005). Investigation of glacial dynamics in Lambert Glacial Basin using satellite remote sensing techniques.
493 (PhD), Texas A&M University, College Station, TX.
- 494
- 495 Yu, J. Y., Liu, H. X., Jezek, K. C., Warner, R. C., & Wen, J. H. (2010). Analysis of velocity field, mass balance, and
496 basal melt of the Lambert Glacier-Amery Ice Shelf system by incorporating Radarsat SAR interferometry and ICESat
497 laser altimetry measurements. *Journal of Geophysical Research-Solid Earth*, 115, doi:Artn
498 B1110210.1029/2010jb007456.
- 499

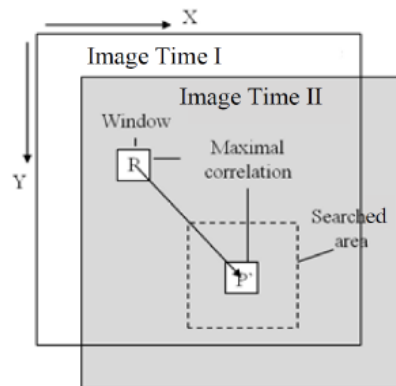


500 Zhang, S. K., Dongchen, E., Wang, Z. M., Li, Y. S., Jin, B., & Zhou, C. X. (2008). Ice velocity from static GPS
501 observations along the transect from Zhongshan station to Dome A, East Antarctica. *Annals of Glaciology*, Vol 48,
502 48, doi: 10.3189/172756408784700716.
503
504 Zhou, C. X., Zhou, Y., Deng, F. H., Ai, S. T., Wang, Z. M., & E, D. C. (2014). Seasonal and interannual ice velocity
505 changes of Polar Record Glacier, East Antarctica. *Annals of Glaciology*, 55(66), 45-51,
506 doi:10.3189/2014AoG66A185.

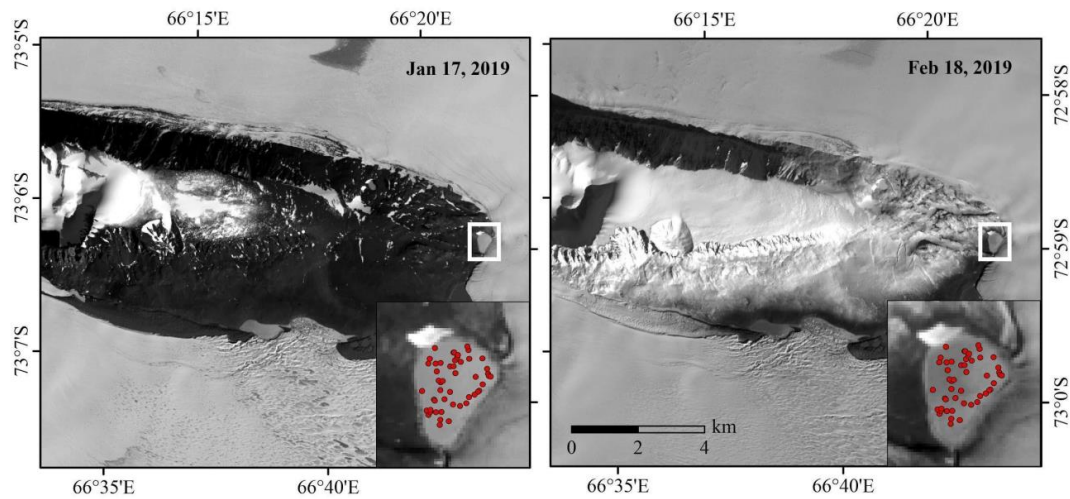


507
508 **Figure 1: Location of southern segmentation of the AIS grounding line (~76 km in length) highlighted in bold black line.**
509 **The background image is the InSAR-derived ice velocity map (Rignot et al., 2017) masked by the basin boundaries. The**
510 **black box represents the location of the study area. The red star is the location selected for uncertainty assessment (Fig 3).**
511 **The red box in the inset map shows the location of Fig 1.**

512
513

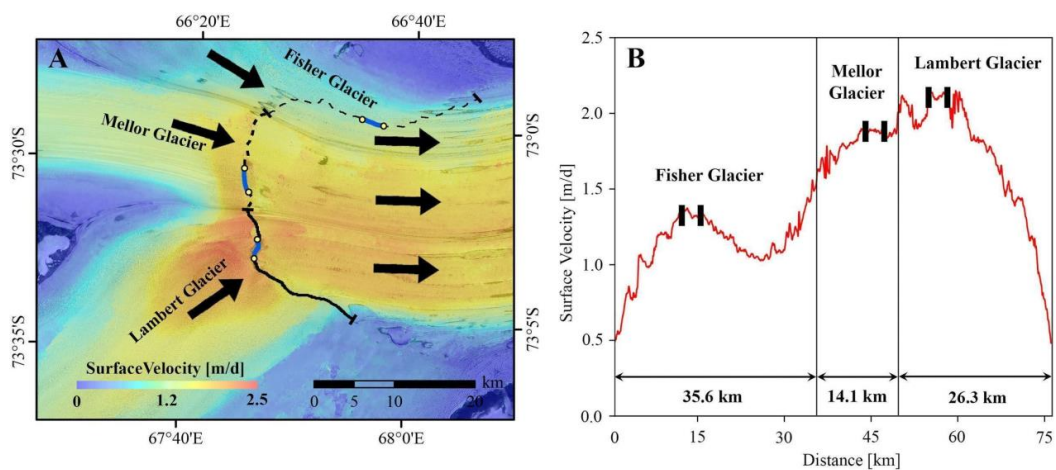


514
515 **Figure 2: Sketch map illustrating feature tracking (Chi, 2012).**



516
517 **Figure 3: The location used for uncertainty assessment is highlighted in white box superimposed on the Landsat-8 OLI**
518 **band 8 image acquired on January 17, 2019 (Left) and on February 18, 2019 (Right). The inset maps illustrate the fifty**
519 **random locations generated for uncertainty assessment. The location of Fig 3 has also been shown in Fig 1.**

520
521



522

523

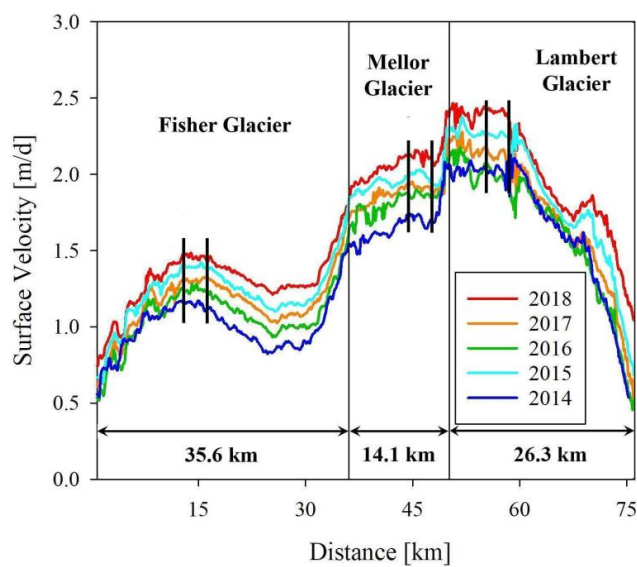
524

525

526

527

Figure 4: (A) Grounding line segments corresponding to the Fisher Glacier, Mellor Glacier, and Lambert Glacier are illustrated using different line symbols superimposed on the feature tracking-based surface velocity map using Landsat-8 OLI image pair of 01/17/2019 and 02/18/2019. Black arrows represent the ice flow direction. (B) The corresponding surface velocity profile along the studied grounding line segmentation. The grounding line segments highlighted in blue (Fig 4A) correspond to the black parallel lines representing the peak velocity locations.

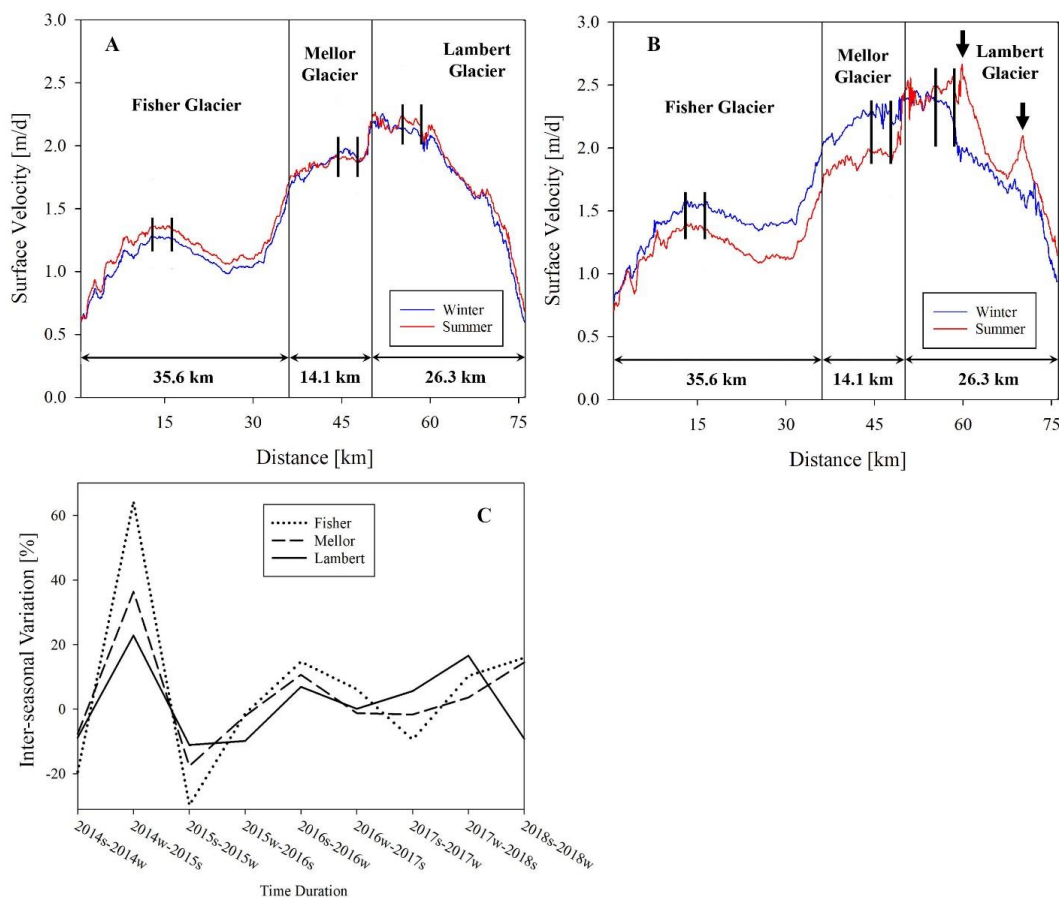


528

529

530

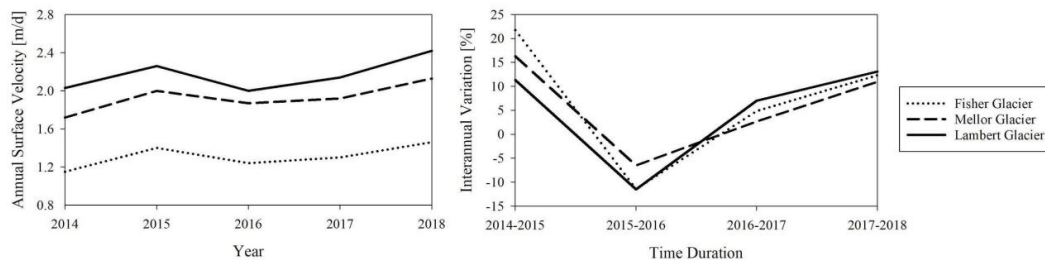
Figure 5: Surface-parallel annual surface velocity during 2014–2018. Black parallel lines represent the peak velocity location for each studied glacier.



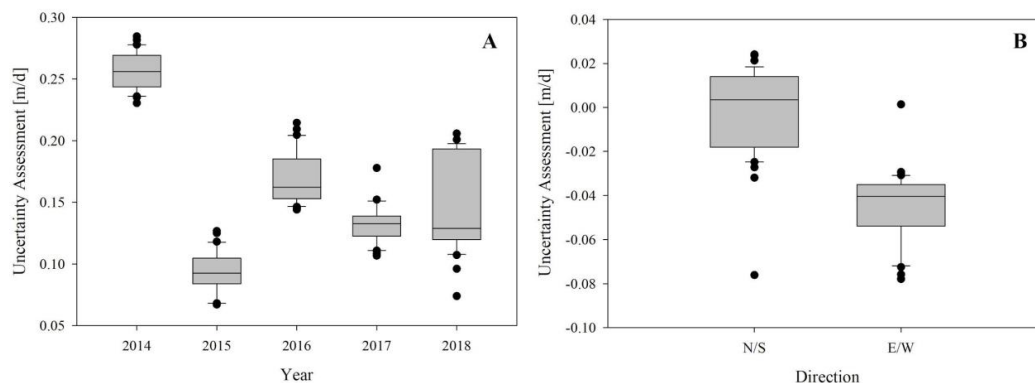
531
 532 **Figure 6: Surface velocity profiles of (A) multiyear average for the summers and winters, (B) the year of 2018,**
 533 **and (C) the inter-seasonal variations for five consecutive summers and winters during 2014–2018. Note the x-**
 534 **axis label in Fig 6c represents prior-current season. Black arrow indicates the new region of increased velocity**
 535 **identified by this study.**

536

537



538
 539 **Figure 7. (A) Annual surface velocity and (B) inter-annual surface velocity variation at the peak velocity**
 540 **location for the three studied glaciers.**

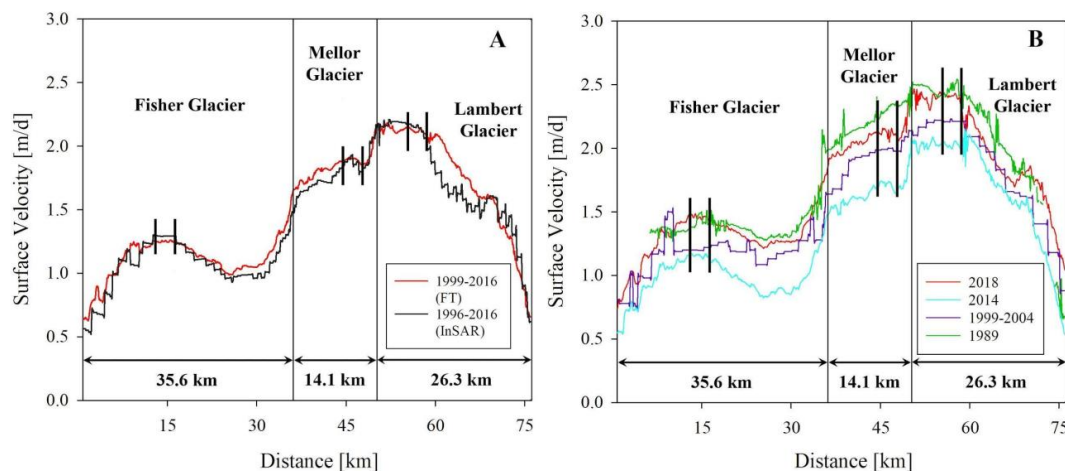


541

542 **Figure 8: The uncertainty assessment represented by the box-and-whisker chart (A) for each year and (B) along**
 543 **N/S and E/W directions respectively during 2014–2018.**

544

545



546

547 **Figure 9: Comparisons of surface velocity (A) of the multiyear mean estimates between the feature tracking**
 548 **velocity and the MEaSURE InSAR velocity at version 2 (Rignot et al., 2017), and (B) of the multi-temporal**
 549 **annual estimates derived using feature tracking alone. Note that the historical surface velocities (1989 & 1999–**
 550 **2004) were provided by Chi’s dissertation work (2012). FT stands for feature tracking.**

551



552 **Table 1: List of Landsat-8 OLI image pairs acquired for feature tracking.**

Pair	Pre-Date	Post-Date	Time Interval (d)
1	01/17/2019	02/18/2019	32
2	09/27/2018	10/22/2018	25
3	01/23/2018	02/22/2018	30
4	09/17/2017	10/26/2017	39
5	01/27/2017	02/28/2017	32
6	09/21/2016	10/23/2016	32
7	02/17/2016	03/13/2016	25
8	10/05/2015	11/13/2015	39
9	01/22/2015	03/02/2015	39
10	10/09/2014	11/19/2014	41
11	02/02/2014	02/27/2014	25

553

554

555 **Table 2: Inter-annual variations of peak surface velocity for each studied glacier (m/d).**

Year	Fisher	Mellor	Lambert	Mean±Stdev
2014/2015	0.24±0.02	0.29±0.02	0.23±0.01	0.25±0.02
2015/2016	-0.15±0.02	-0.13±0.02	-0.26±0.04	-0.18±0.03
2016/2017	0.06±0.02	0.05±0.02	0.13±0.04	0.08±0.03
2017/2018	0.16±0.01	0.20±0.03	0.28±0.02	0.21±0.02
Mean±Stdev.	0.08±0.02	0.10±0.02	0.10±0.03	0.09±0.02

556

557 **Table 3: Intra-annual variation of surface velocity for each studied glacier (m/d).**

Year	Fisher	Mellor	Lambert	Mean±Stdev
2014	-0.21±0.06	-0.13±0.09	-0.16±0.21	-0.17±0.12
2015	-0.42±0.04	-0.38±0.09	-0.22±0.09	-0.34±0.07
2016	0.15±0.05	0.18±0.12	0.11±0.15	0.15±0.11
2017	-0.11±0.07	-0.03±0.07	0.10±0.09	-0.01±0.08
2018	0.19±0.08	0.28±0.08	-0.19±0.17	0.09±0.11
Mean±Stdev.	-0.08±0.06	-0.02±0.09	-0.07±0.14	-0.06±0.10



558

559 **Table 4: Intra-annual and inter-annual surface velocity variations for three studied glaciers.**

Year	Intra-annual Variation (%)				Inter-annual Variation (%)			
	Fisher	Mellor	Lambert	Mean	Fisher	Mellor	Lambert	Mean±Stdev
2014	-19.13 ±5.58	-7.66 ±5.62	-10.62 ±16.79	-12.47 ±9.33				
2015	-30.32 ±4.51	-17.56 ±4.48	-11.71 ±5.66	-19.86 ±4.88	25.02 ±5.13	19.63 ±4.70	11.52 ±6.05	18.72 ±5.29
2016	15.79 ±7.38	11.07 ±6.25	8.96 ±10.31	11.94 ±7.98	-13.06 ±3.39	-6.86 ±4.11	-13.33 ±7.95	-11.08 ±5.15
2017	-9.17 ±4.25	-1.73 ±3.84	6.33 ±7.24	-1.52 ±5.11	8.44 ±4.24	2.96 ±3.48	7.73 ±7.75	6.38 ±5.15
2018	15.77 ±6.54	14.66 ±4.34	-9.34 ±7.33	7.03 ±6.07	13.83 ±4.69	10.15 ±1.65	17.24 ±15.06	13.74 ±7.13
Mean ±Stdev	-5.41 ±5.65	-0.24 ±4.90	-3.28 ±9.47	-2.98 ±6.67	8.56 ±4.36	6.47 ±3.48	5.79 ±9.20	6.94 ±5.68

560

561 **Table 5: SNR of surface velocity measurements along the southern grounding line of AIS during 2014–2018.**

562 **OA stands for overall accuracy.**

Year	Summer	Winter	Annual
2014	0.9692	0.9730	0.9711
2015	0.9601	0.9658	0.9630
2016	0.9744	0.9603	0.9674
2017	0.9630	0.9612	0.9621
2018	0.9542	0.9704	0.9623
OA	0.9642	0.9661	0.9652

563